Improving Horizontal Stabilizer Performance Using Aeroelastic Tailoring

R.C.M. Cheung[1], D. Rezgui[2] and J.E. Cooper[3]
Department of Aerospace Engineering, University of Bristol, University Walk, Bristol, BS8 1TR, UK.

and
R.B. Green[4]
University of Glasgow, Aerospace Sciences, James Watt Building South, Glasgow G12 8QQ, UK.

and
R.C. Llamas-Sandin[5]
AIRBUS OSL, Av. John Lennon s/n, 28096 Getafe, Spain.

Horizontal stabilizers fitted to conventional passenger jets typically exhibit increased washout under aerodynamic load. Such aeroelastic behavior reduces the lift generated by the stabilizers and the achievable lift-curve slope. In order to satisfy control and stability requirements, this loss of performance is often compensated by increasing the size and structural stiffness of the stabilizers, both of which add to the overall aircraft weight. This work explores using aeroelastic tailoring to minimize such a performance deficit by considering the optimal skin layup for inducing a favorable static aeroelastic response. This paper reports on the design and vibration testing of a wind tunnel prototype of such construction, intended to experimentally demonstrate the improvement achieved in the forward, backward and zero-sweep configurations.

I. Introduction

In a conventionally configured aircraft, the lift-curve slope of the horizontal stabilizers directly affects stability of the aircraft. Since a reduction in the lift-curve slope is often observed under aerodynamic load due to aeroelastic coupling, the size of the stabilizers must increase to meet the performance set by certification requirements[1], which adds to overall drag and weight of the aircraft.

Since the lift-curve slope reduction observed is an aeroelastic effect, this shortcoming may be addressed through modifying the underlying structure of the stabilizer to achieve the desired behavior. This process may be described as aeroelastic tailoring, which has the goal of optimizing directional stiffness in the aero-structure for aeroelastic benefits[2]. Modern application of aeroelastic tailoring often refers to optimizing the layup of the laminated composite used, through exploiting the anisotropic property of the constituent components. Unidirectional fiber laminates are typically used because of this property, and thus the desired directional stiffness can be more readily achieved by optimizing the total number of plies and their individual orientation. This is a well-studied technique which has featured in several works focusing on aircraft wings, demonstrating enhancements ranging from reduced gust loads[3] to increased aileron reversal speed[4]. However, documented application to the horizontal stabilizer remains limited, hence the current work is motivated to further this knowledge.

---

[1] Research Associate, Department of Aerospace Engineering.
[2] Senior Lecturer in Aerospace Engineering, Department of Aerospace Engineering, MAIAA.
[3] Airbus Royal Academy of Engineering Sir George White Professor of Aerospace Engineering, FAIAA.
[4] Senior Lecturer in Aeronautics, Aerospace Sciences Division.
[5] Future Projects Engineer.

In this work, a wind tunnel prototype of a horizontal stabilizer is constructed following an aeroelastic optimization process for improved lift-curve slope. It is commonly known that wing sweep has a large influence on static aeroelastic behavior, therefore the wind tunnel prototype is intended to be additionally tested in the forward and backward swept configurations. This paper describes the design and manufacturing process and the results from the vibration tests, as well as the numerical predictions.

II. Wind Tunnel Model

A. Design

The wind tunnel model is a 1.6m semispan horizontal stabilizer. As shown in Figure 1, it consists of five main components: wing box, leading edge, trailing edge, wingtip and the wing-root covers. The leading and trailing edge parts are designed to transfer the aerodynamic load on the wing box without adding a significant contribution to the overall stiffness of the aerodynamic surface. Therefore, these two parts have cuts in multiple spanwise stations to reduce their stiffness contribution. The wing box is a major contributor to the overall stiffness and thus it is the subject of the aeroelastic tailoring process, in which an optimized composite layup is used as its exterior together with a foam core. A total of two wing boxes are manufactured, with one designated 'black-metal' as the un-optimized reference model. Together with a custom wing-root attachment for forward, backward and zero-sweep configuration, these two models will allow the benefits of aeroelastic tailoring to be established for all three sweept configurations.

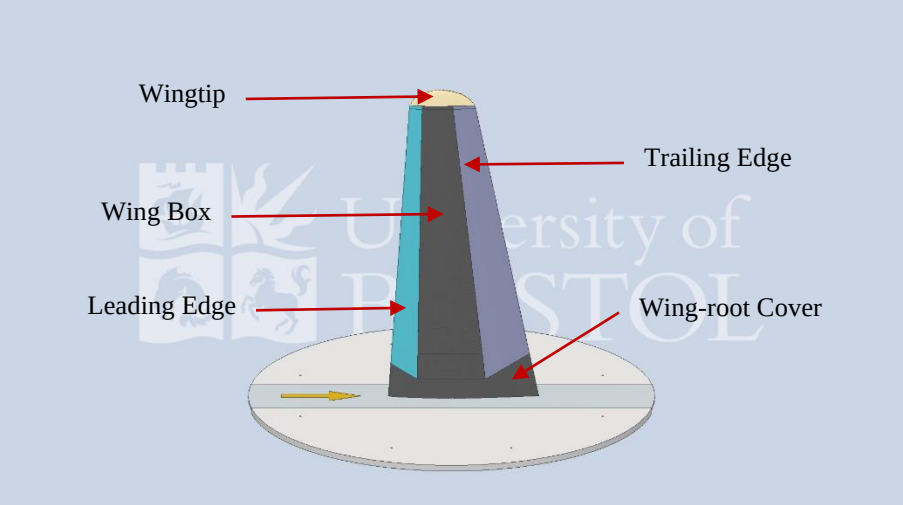

Figure 1 Wind tunnel model.

B. Wind Tunnel Testing

Wind tunnel testing is scheduled to be carried out in the de Havilland Wind Tunnel at the University of Glasgow early 2022. The wind tunnel model is oriented vertically to the turntable, as illustrated in Figure 1. A 30-deg forward and a 30-deg backward swept configuration are tested in additional to the reference 'zero-sweep' configuration shown. In all configurations, the test campaign covers a wide range of incidence and wind tunnel velocity up to 50m/s.

III. Aeroelastic Tailoring

Aeroelastic tailoring is carried out using Nastran as the analysis tool. This allows the composite skin layup to be modelled in a finite element model (FEM), such that the optimal ply orientation and coverage can be determined based on the resulting aeroelastic prediction. Figure 2 shows the outer shell that models the composite layup and hexahedral elements for the foam core on the interior. The aerodynamics is modelled using the Doublet Lattice Method (DLM)[5] and the input meshes for all sweep configurations are shown in Figure 3.

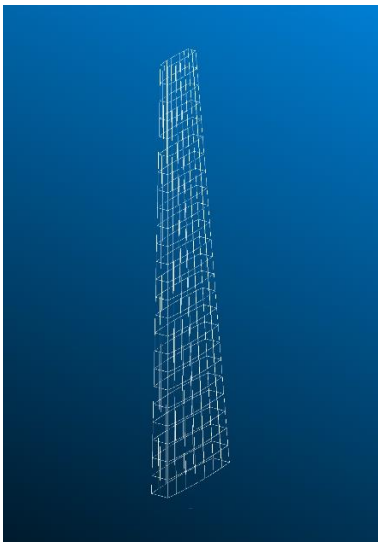

(a) Skin

(b) Foam core

Figure 2 Wing box FEM.

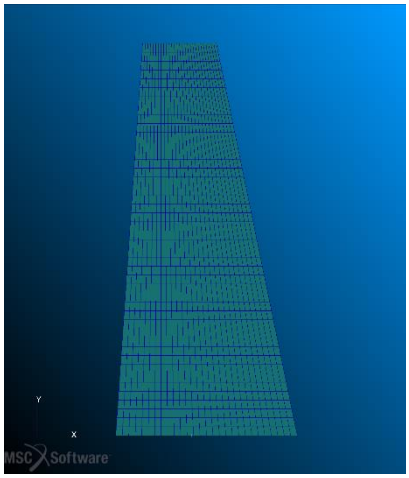

(a) Zero-sweep

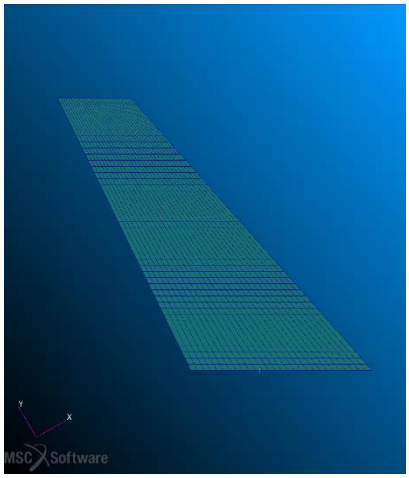

(b) 30-deg forward-swept

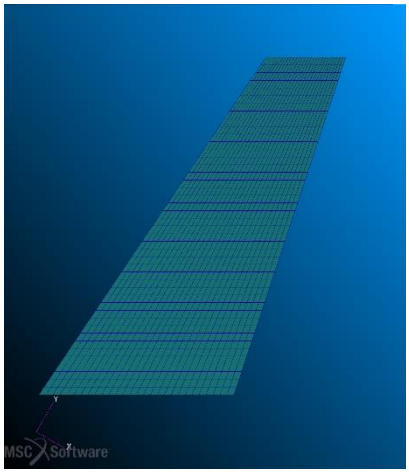

(c) 30-deg backward-swept

Figure 3 DLM panels.

The wing box is constructed from composite fabric wrapped over a central foam core as illustrated in Figure 4. The front and rear spar structures are manufactured using Hexforce G0904 D 1070. The skins are made using AIMS 05-04-100, which is a carbon fiber fabric of high stiffness in the warp direction. The anisotropic nature of this fabric allows the global stiffness of the skin to be varied through its orientation, and thus providing the means of aeroelastic tailoring. Fiber orientation or ply-angle for this work is defined relative to the 50% chord line along the span of the wing box, and clockwise-positive when viewed from the outside of the structure.

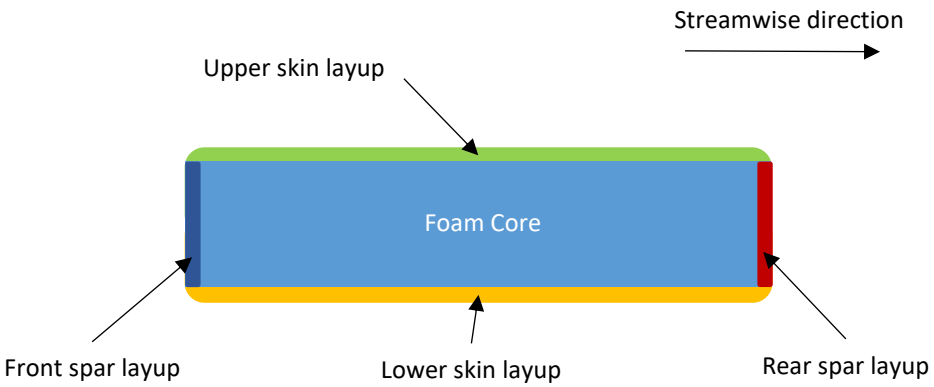

Figure 4 Wing box cross-section.

The materials used are listed in Table 1, in which the listed stress limits have been reduced from the manufacturer's specification to account for manufacturing variability.

Table 1 Composite materials.

Material	Foam core	Skin ply	Spar ply
Type	UNE EN 13164	AIMS 05-04-100	Hexforce G0904 D 1070
Ply thickness (cured), mm	-	0.262	0.2
Density, kg/m^3	39	1600	1530
Tensile allowable stress, MPa	0.5	Warp direction: 1160 Weft direction: 32	Fiber direction: 700
Compressive allowable stress, MPa	0.3	Warp direction: 308 Weft direction: 70	Fiber direction: 670
Elastic modulus, GPa	0.013	Warp direction: 130 Weft direction: 9.5	Fiber direction: 65
In plane shear strength, MPa	0.2	80	80
In plane shear modulus, GPa	0.0045	4	4

A. Black-metal model

The black-metal model is a reference model to be used for comparison purposes. It is constructed using a single ply for each spar at 45 deg ply-angle and two plies for each skin, which are both oriented at zero ply-angle.

B. Aeroelastically-tailored model

The aeroelastically-tailored model is similar to the black-metal model, in that a single ply at 45 deg ply orientation is used for each spar as well. The difference between the two models lies in the layup for each skin, as determined through the aeroelastic tailoring process detailed below.

Utilizing the gradient-based optimization routine built into Nastran, SOL200, the aeroelastic FEM is optimized to maximize lift difference between two angles of attack, which is equivalent to maximizing the lift-curve slope of the horizontal tail. The two chosen conditions are positive and negative 10-deg angle of attack at 50m/s. A safety factor of 2.0 based on the Tsai-Hill failure criterion[6] is also specified as stress constraint.

Initial calculations indicated that the optimum solution requires between one and two skin plies. Therefore, the optimization is formulated based on the skin layup in Figure 5, with the optimizer tasked to find the best combination of ply angles and inner ply span. In order to carry out these tasks using Nastran SOL200, global optimization is split into local cases, in which each local case is an optimization run for finding the optimal ply orientation for maximum lift-curve slope, for a given combination of upper and lower skin inner ply span. The inner ply ranges from zero-span to covering all 24 spanwise zones, according to the zone boundaries seen in Figure 6.

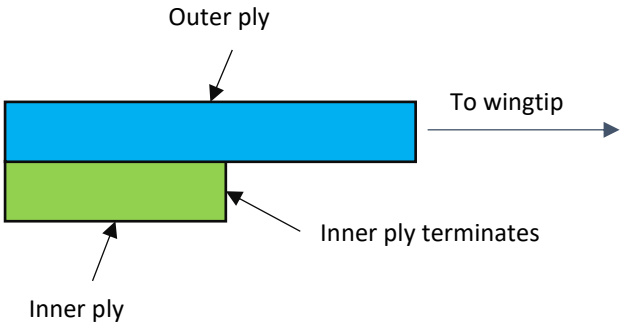

Figure 5 Ply layup.

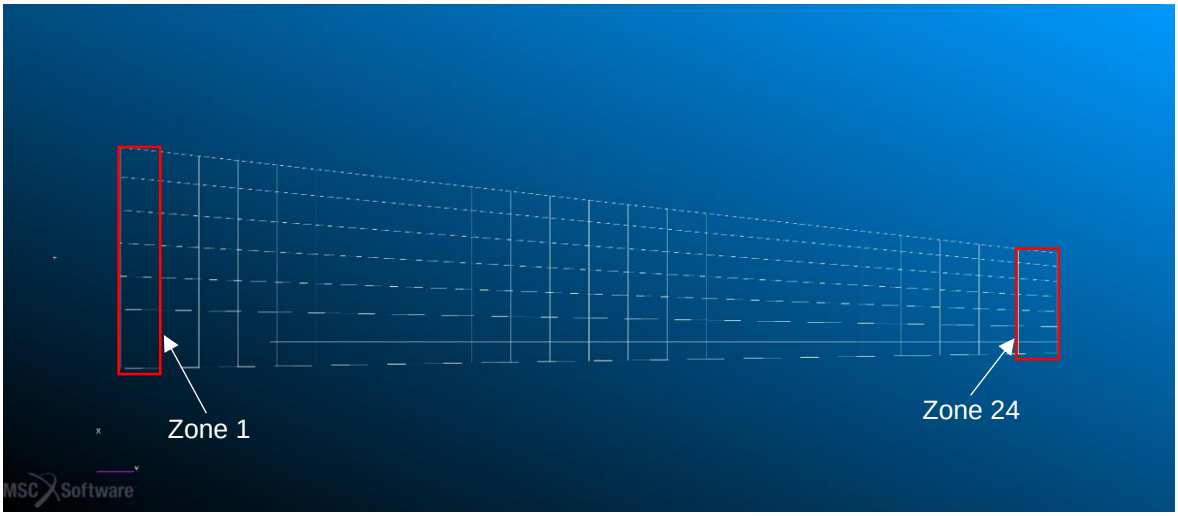

Figure 6 FEM regions.

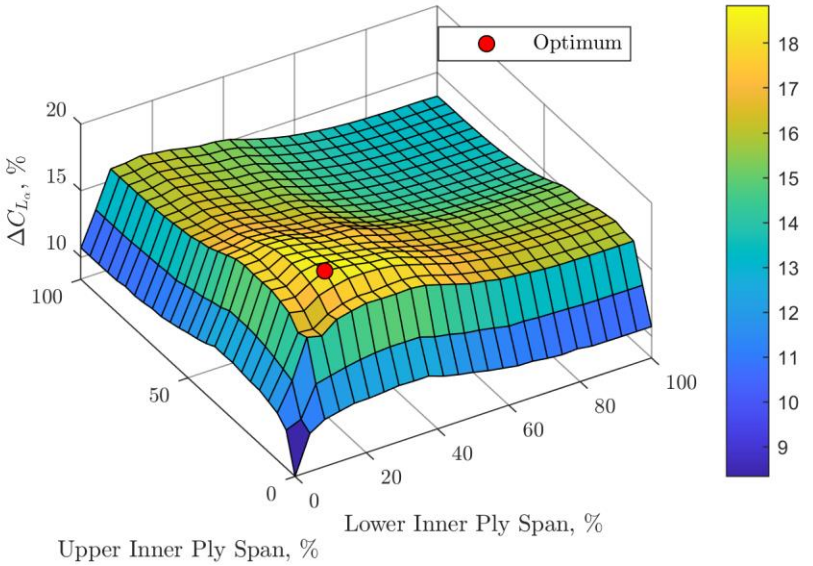

Figure 7 Response surface of lift-curve slope change against inner ply span.

Table 2 Comparison of optimization results for the 30-deg forward-swept configuration.

	Black-metal	Aeroelastically-tailored
Lift-curve slope, rad^{-1}	3.763	4.472 (+18.8%)
Upper skin inner ply span, %	100.0	20.8
Upper skin outer ply θ, deg	0.0	-23.1
Upper skin inner ply θ, deg		-19.6
Lower skin inner ply span, %	100.0	20.8
Lower skin outer ply θ, deg	0.0	23.1
Lower skin inner ply θ, deg		19.6

By collating the optimal solution in each local case, a response surface is constructed as shown in Figure 7, allowing the global optimum to be identified. As shown in Table 2, in the 30-deg forward-swept configuration, the aeroelastically-tailored wind tunnel model is predicted to improve the flexible lift-curve slope by 18.8% when compared to the black-metal reference. Through comparing the spanwise twist distribution, it can be seen in Figure 8 that aeroelastic tailoring has induced a higher level of wash-in to achieve the gain in lift.

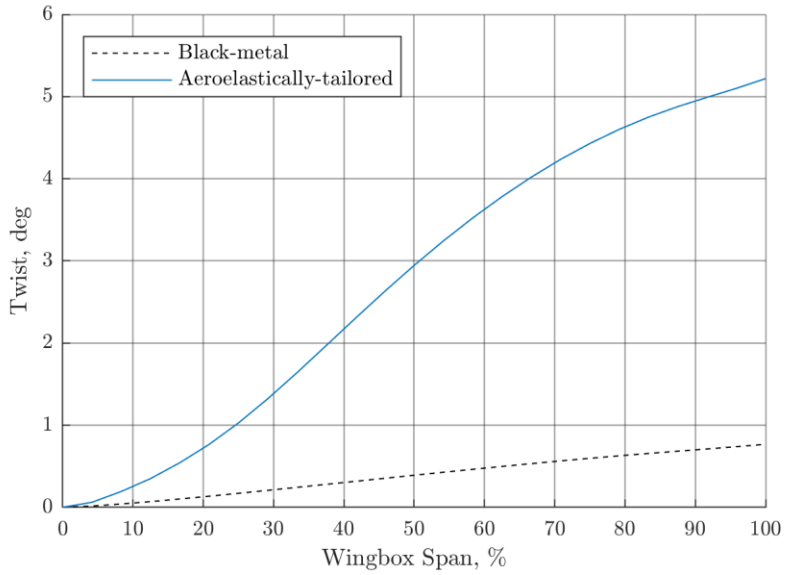

Figure 8 Wing twist at 50m/s with 10-deg angle of attack in the 30-deg forward-swept configuration.

C. Static aeroelastic performance

In the aeroelastic tailoring process, only the forward-swept configuration was considered as it presented the opportunity for the best possible performance gain. Therefore, it is necessary to further analyze the static aeroelastic performance of the wind tunnel models in the remaining sweep configurations. The analysis is performed using NASTRAN SOL144 with a 10-deg angle of attack at wind tunnel velocity of 50 m/s, which is the same as the reference condition used in the previous aeroelastic optimization. As shown in Table 3, the aeroelastically-tailored model is predicted to retain an improved lift-curve slope in all sweep configurations. It should be noted that the lift-curve slope calculation is performed using the standardized reference wing area of $0.8320m^2$ and the backward-swept configuration has a higher baseline lift-curve slope than the forward-swept configuration because of its higher effective aspect ratio.

Table 3 Static aeroelastic performance prediction at 10-deg angle of attack and wind tunnel velocity of 50 m/s.

Sweep, deg	Effective Aspect Ratio	DLM Wing Area, m^2	Black-metal		Aeroelastically-tailored		Difference
			Lift, N	Lift-curve Slope, rad^{-1}	Lift, N	Lift-curve Slope, rad^{-1}	
-30	4.28	0.8644	836.75	3.763	994.39	4.472	+18.8%
0	6.15	0.8320	1017.74	4.577	1184.01	5.325	+16.3%
30	4.90	0.8125	849.57	3.821	894.63	4.023	+5.3%

D. Flutter analysis

Flutter analysis is carried out to assess the dynamic behavior of the wind tunnel models. This task is carried out as a safety check to ensure flutter does not occur at any part of the test campaign. The analysis is performed using the FEM described previously and through NASTRAN SOL145 via PK method.

For these computations, a lumped mass of 0.387kg is added to the wingtip region of the FEM to represent the mass of the physical wingtip. As an additional margin of safety, the structural damping parameter is reduced to 1%, from a value of 2% that is conventionally used in structural dynamics.

For the black-metal model, aeroelastic instability in the form of divergence is predicted to occur beyond 225m/s, in the forward-swept and zero-sweep configurations, as shown in Figure 9(a) and Figure 10(a) respectively. In the backward-swept configuration, the limiting aeroelastic instability is flutter, which is predicted to occur far beyond the intended wind tunnel test velocity, at 265m/s as indicated in Figure 11(a).

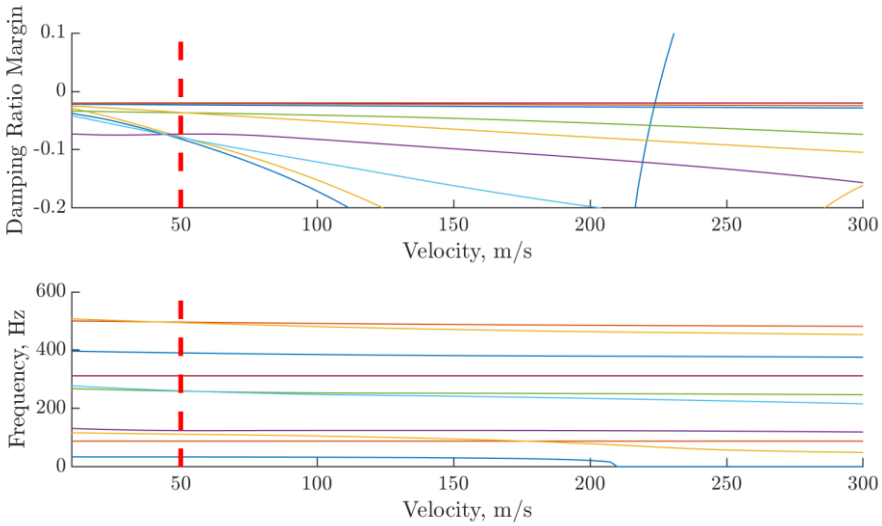

(a) Black-metal

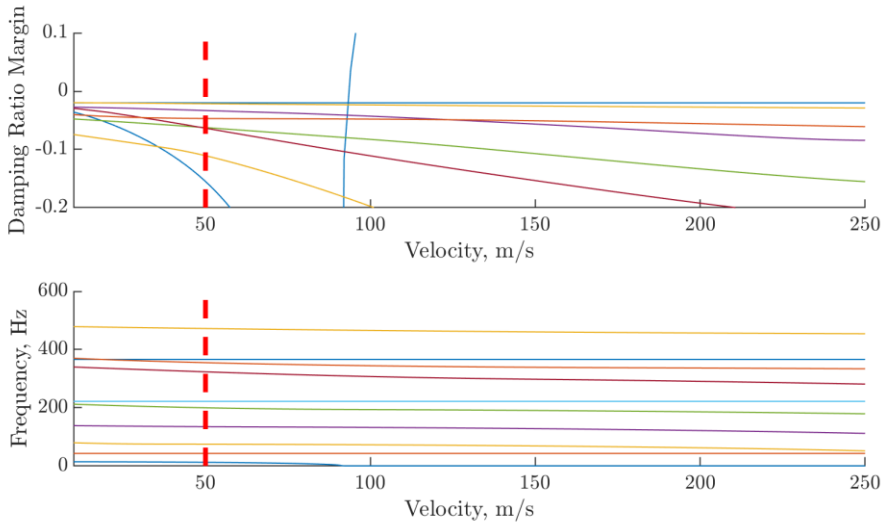

(b) Aeroelastically-tailored

Figure 9 Flutter analysis results – 30-deg forward-swept (maximum test velocity in red broken line).

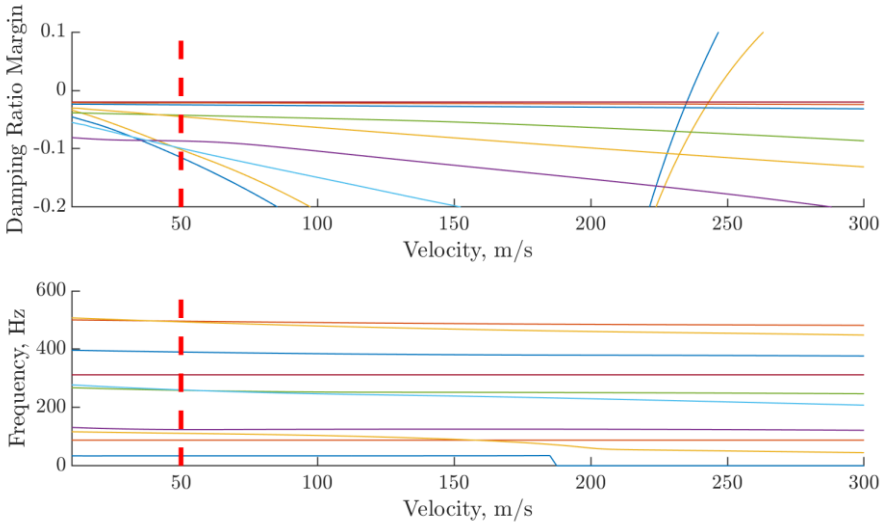

(a) Black-metal

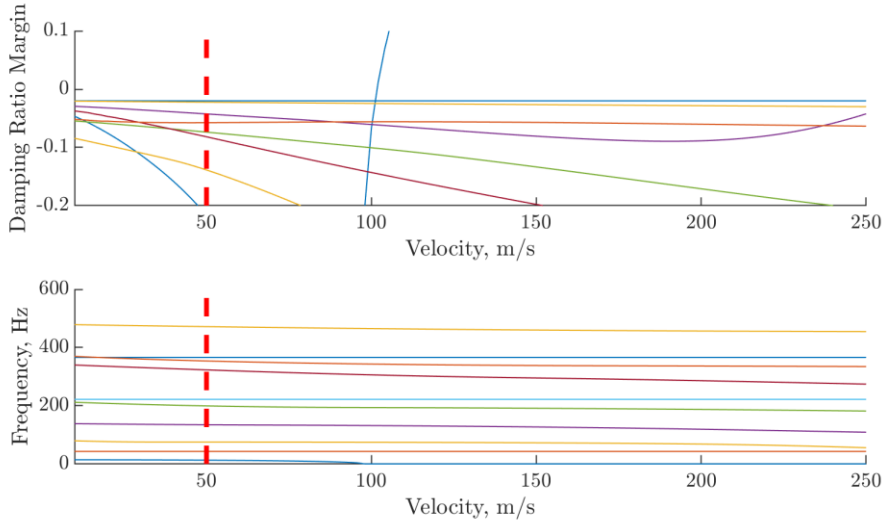

(b) Aeroelastically-tailored

Figure 10 Flutter analysis results – zero-sweep (maximum test velocity in red broken line).

The limiting aeroelastic instability for the aeroelastically-tailored model is divergence. The limiting velocities range from 93m/s in the forward-swept configuration as shown in Figure 9(b), to 185m/s in the backward-swept configuration as seen in Figure 11(b). This reduction in divergence velocity compared with the black-metal model is within expectation, because aeroelastic tailoring has been used to promote bend-twist coupling of the wing, which is directly related to the mode that exhibits divergence in these conditions.

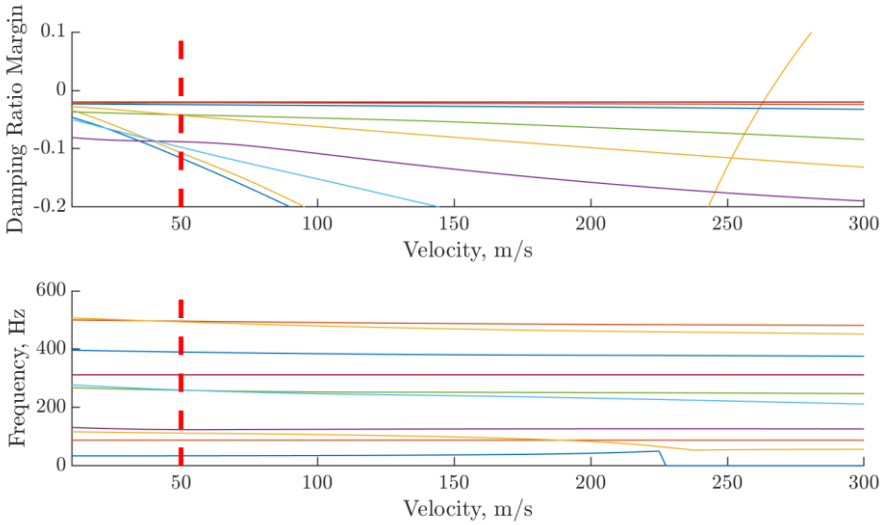

(a) Black-metal

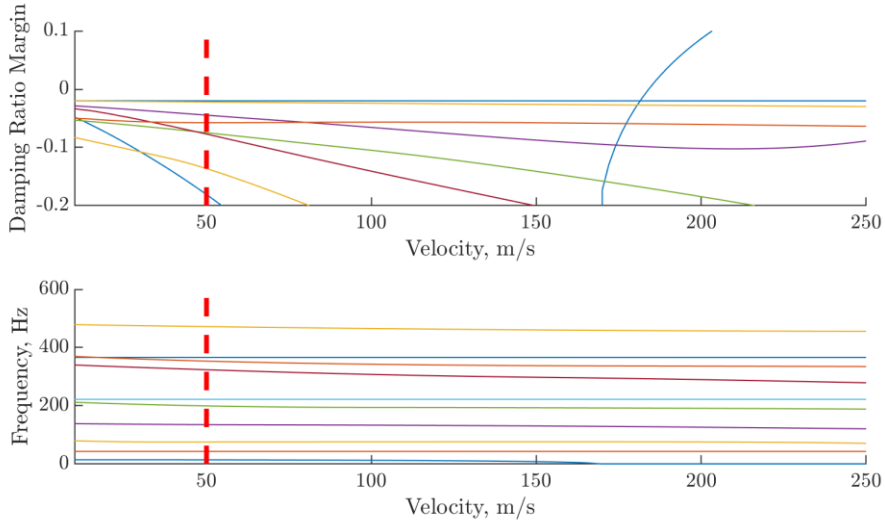

(b) Aeroelastically-tailored

Figure 11 Flutter analysis results – 30-deg backward-swept (maximum test velocity in red broken line).

As already seen from Figure 9 to Figure 11, the damping ratio margins for both models are negative for all speeds leading up to the intended maximum test velocity of 50m/s and remain negative until the instability velocities mentioned above. This means all the analyzed aeroelastic modes are dynamically stable and the wind tunnel models are free from aeroelastic instabilities in the intended test conditions.

IV. Vibration Test

Vibration tests are carried out on both the black-metal and the aeroelastically-tailored models. The purpose of the tests is to establish the structural properties of the manufactured wind tunnel models, such that the corresponding FEMs can be updated and thus allowing a more accurate prediction of their aeroelastic behaviors.

Figure 12 Vibration test setup.

In the test configuration shown in Figure 12, the wing box is mounted on a hard wall using the mounting components intended for the wind tunnel test. This setup allows for the effect of these components has on the overall structural behavior to be captured, such that the updated FEMs correspond to a consistent and appropriate boundary condition for wind tunnel test prediction.

In each test, the wing box is excited using a shaker connected to the front spar as shown in Figure 12. The shaker is driven by a LMS SPM50 through an amplifier. This system contains 16 accelerometer channels which are fully populated. The corresponding accelerometers are distributed along the front and rear spar of the wing box, with a tri-axial type located at the front spar near the wingtip. Majority of the accelerometers is orientated to measure in the out-of-plane direction, with two measuring the in-plane direction at the root mount and mid-span. This configuration of accelerometers is more focused on the bending modes of the wing box as they are expected to dominate the lower frequency range. The in-plane measurements are also necessary because of the presence of the first in-plane mode within this frequency range as well. Each shaker test is run with a burst random excitation up to 512Hz and the process is repeated 40 times.

A. Vibration results and FEM updating

The black-metal and aeroelastically-tailored wing box weigh 1.5kg and 1.4kg respectively, and thus the additional weight of the accelerometers is accounted for in the FEM correction process to improve accuracy. The encastre boundary condition at the wing box root is replaced by three tuning beams as shown in Figure 13(b). These beams are used to represent the stiffness of the mounting fixture such that the modeshapes and frequencies can match with those found from the vibration tests.

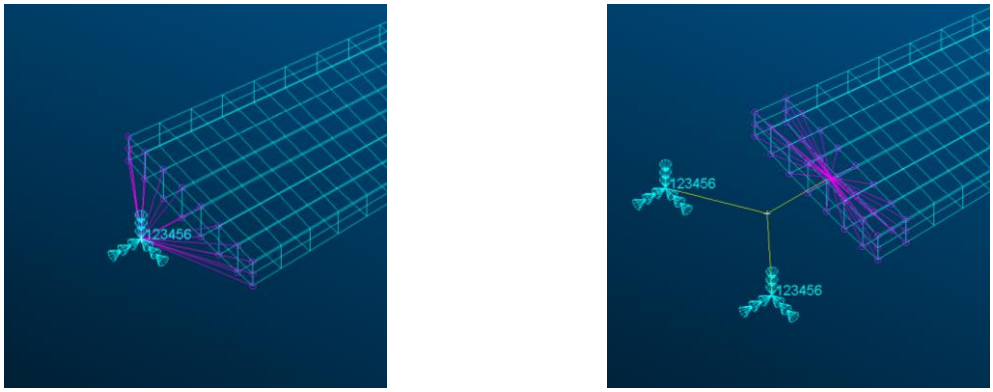

(a) Encastre boundary condition (b) Tuning beams

Figure 13 Boundary conditions used in the FEMs.

The black-metal experimental results were used as the initial target for tuning, and the tuned beams are then used in the aeroelastically-tailored FEM. To assess the correlation of vibration modes between the experiment and the corrected FEM, modal assurance criterion (MAC) is computed. In Figure 14, the black-metal wing box FEM correlates well with the experimental results as intended and the aeroelastically-tailored wing box results also demonstrate good agreement. However, it is noted that there are a few vibration modes from the experiments that are unaccounted for, which may have been caused by interference from the accelerometer cables, as they are not modelled in the FEMs.

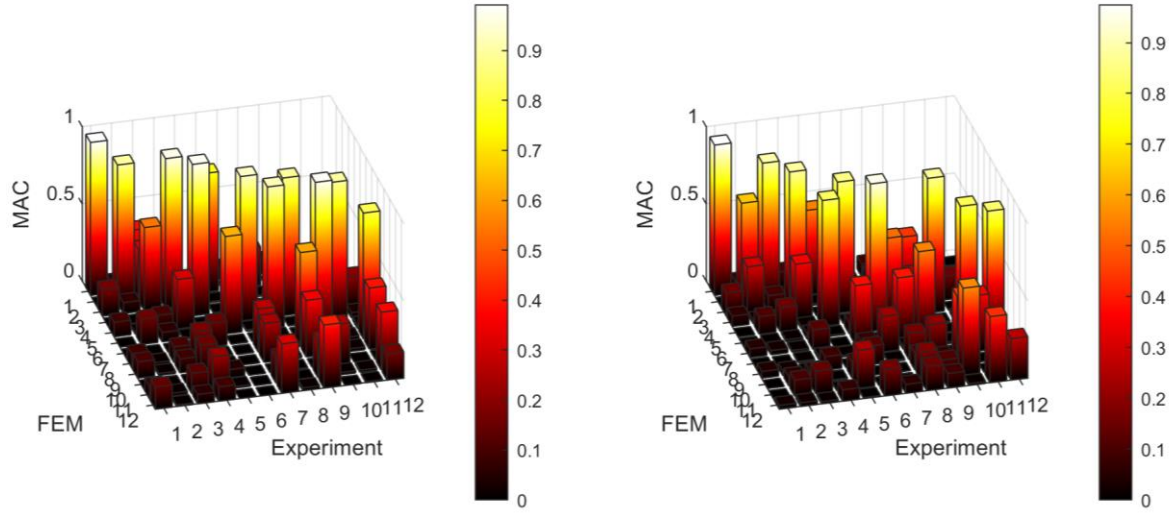

(a) Black-metal (b) Aeroelastically-tailored

Figure 14 Modal assurance criterion between experiment and the corrected FEM.

In the tuning process, the first mode in out-of-plane bending, in-plane bending and torsion are used as targets and thus in Table 4, the modal frequencies from the corrected black-metal wing box FEM match well with the experiment by design. For the aeroelastically tailored wing box, only the first out-of-plane bending and torsion modal frequencies are found to correlate well. Although the discrepancy in the first in-plane bending frequency may be undesirable, the correction is deemed satisfactory because the key mechanism for improving stabilizer performance comes the coupling

between out-of-plane bending and torsion which are already well captured. Comparisons of these key modeshapes are provided in Figure 15 and Figure 16.

Table 4 Comparison of experimental and corrected FEM results.

Mode	Modal Frequency, Hz			
	Black-metal		Aeroelastically-Tailored	
	Experiment (damping)	Corrected FEM	Experiment (damping)	Corrected FEM
1st out-of-plane bending	35.0 (0.46%)	35.4	24.5 (0.56%)	24.3
1st in-plane bending	80.3 (0.92%)	80.6	74.7 (1.53%)	65.2
1st torsion	184.9 (3.29%)	182.9	236.3 (3.42%)	235.5

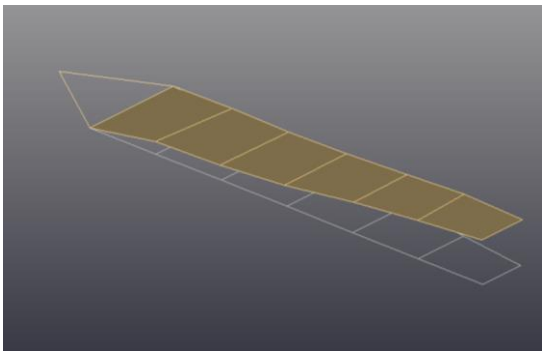

(a) Experiment – out-of-plane bending

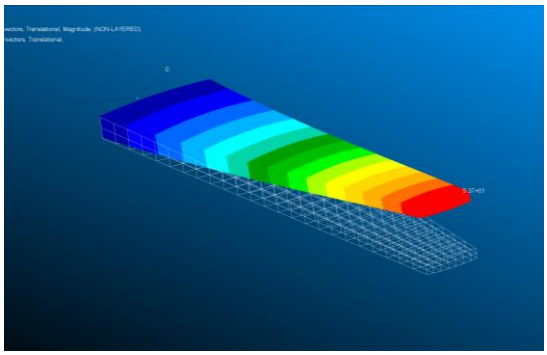

(b) Correct FEM – out-of-plane bending

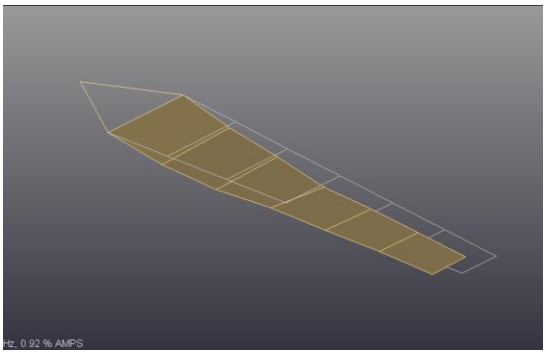

(c) Experiment – in-plane bending

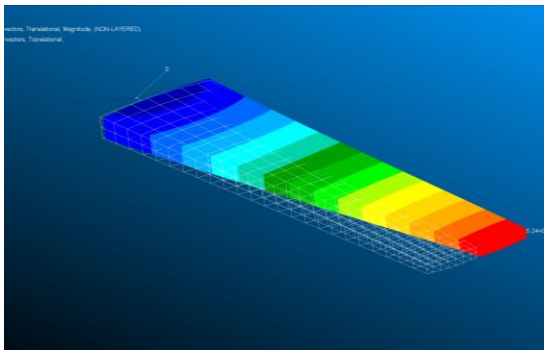

(d) Correct FEM – in-plane bending

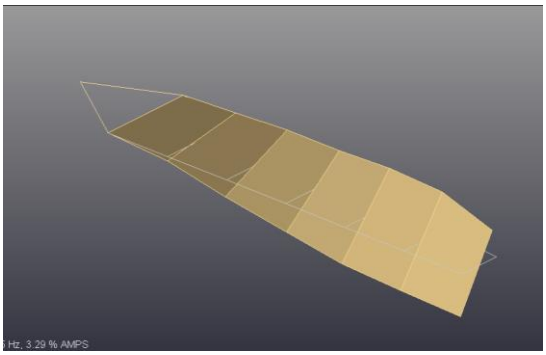

(e) Experiment – torsion

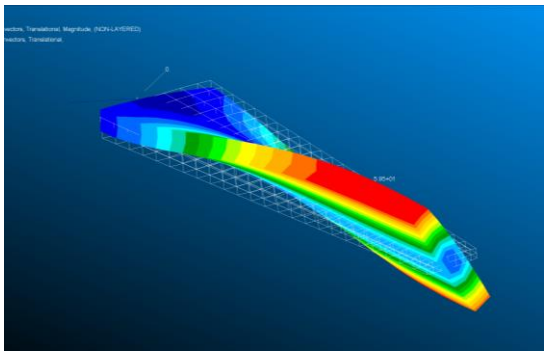

(f) Correct FEM – torsion

Figure 15 Comparison of modeshapes – black-metal wing box.

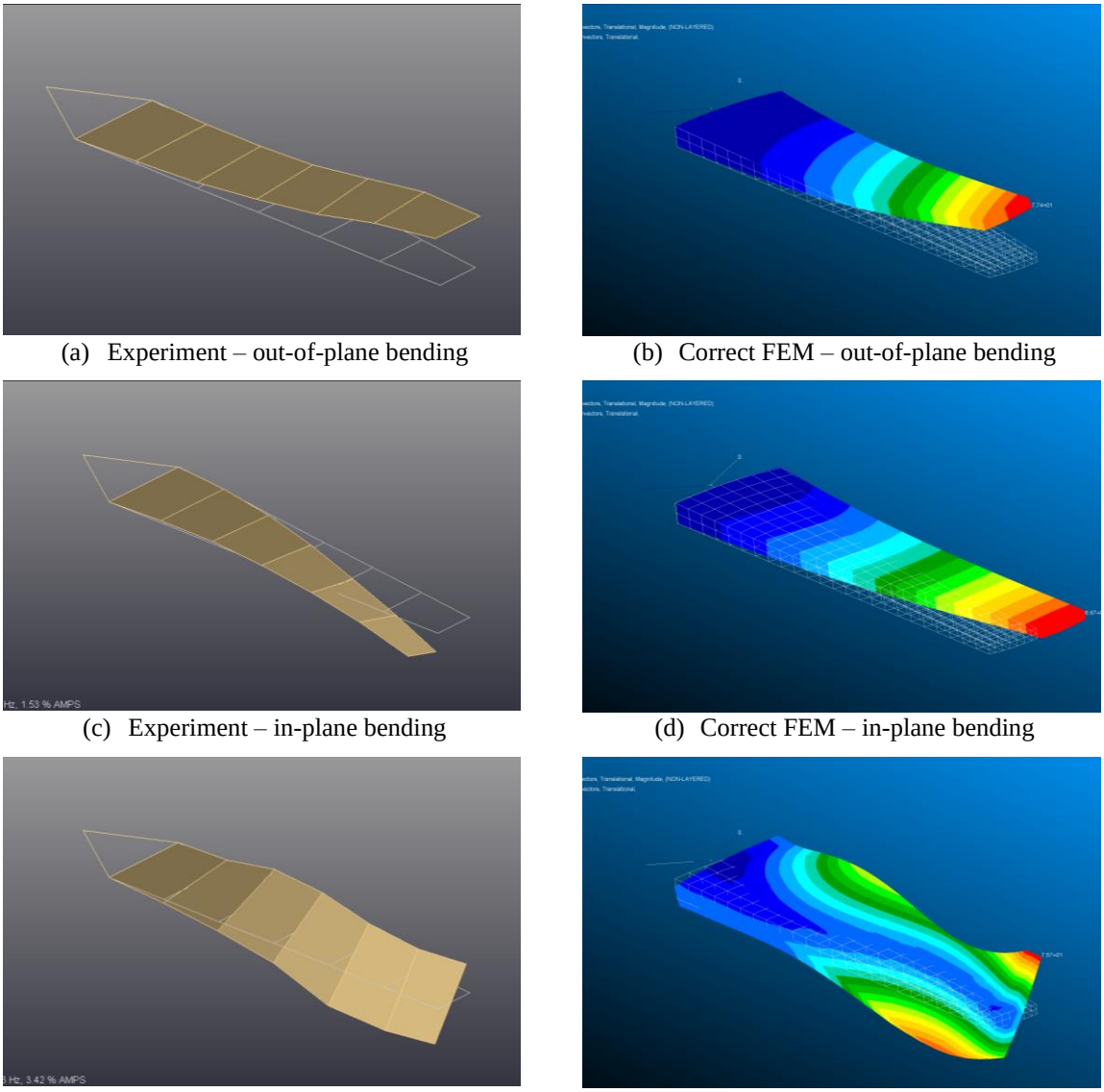

(a) Experiment – out-of-plane bending

(b) Correct FEM – out-of-plane bending

(c) Experiment – in-plane bending

(d) Correct FEM – in-plane bending

(e) Experiment – torsion

(f) Correct FEM – torsion

Figure 16 Comparison of modeshapes – aeroelastically-tailored wing box.

B. Post-correction aeroelastic predictions

Using the corrected FEMs, the static and dynamic aeroelastic predictions are updated. Table 5 shows there is a marginal increase in the predicted static aeroelastic loads for the forward and zero-sweep configurations, when compared to the pre-correction results in Table 3. The main difference between the pre-correction and corrected FEMs is the flexibility of the tuning beams that are introduced, which represent the flexibility of the physical mount. The location of the tuning beams is approximately 42% root chord, which is aft of the expected aerodynamic center for these configurations. Therefore, wash-in can result under lifting load which increases the achieved lift. The reversed is observed in the backward sweep configuration, which further supports this explanation. Across all sweep configurations, the black-metal and the aeroelastically-tailored wing box has an approximately 1% reduction in lift-curve slope difference post-correction.

Table 5 Post-correction static aeroelastic prediction at 10-deg angle of attack and wind tunnel velocity of 50 m/s.

Sweep, deg	Effective Aspect Ratio	DLM Wing Area, m^2	Black-metal		Aeroelastically-tailored		Difference
			Lift, N	Lift-curve Slope, rad^{-1}	Lift, N	Lift-curve Slope, rad^{-1}	
-30	4.28	0.8644	850.64	3.825	1000.15	4.498	+17.6%
0	6.15	0.8320	1019.39	4.584	1171.44	5.268	+14.9%
30	4.90	0.8125	834.46	3.753	874.41	3.933	+4.8%

Divergence continues to be the type of aeroelastic instability of interest post-correction. As shown in Table 6, the divergence speed margin in most configurations is reduced with the introduction of tuning beams into the correct FEM. This observation aligns with the previous explanation regarding the chordwise location of the tuning beams and thus the wash-in that can result. For the aeroelastically-tailored wing box, the flexibility in the tuning beams, and thus the corresponding flexibility in the physical mount, in fact benefits divergence with a small increase in the backward and zero-sweep configurations.

Table 6 Comparison of divergence speed upon FEM correction.

Sweep, deg	Divergence Speed Margin			
	Black-metal		Aeroelastically-tailored	
	Pre-correction	Corrected FEM	Pre-correction	Corrected FEM
-30	77.8%	74.2%	46.5%	46.2%
0	78.9%	78.1%	50.9%	51.7%
30	81.2%	80.9%	72.8%	77.1%

V. Conclusions

An aeroelastically tailored wing tunnel model of a horizontal stabilizer has been designed and manufactured. The wind tunnel model is of an optimized composite construction with the aim of increasing its lift-curve slope and thus its performance as a horizontal stabilizer. A custom test fixture has also been built for wind tunnel testing in the forward, zero and backward sweep configurations to examine the effect of planform variation. Vibration tests have been carried out on the manufactured model as well as a reference, un-optimized model to update their corresponding finite element model. Aeroelastic predictions are performed using these finite element models, in which divergence is predicted to occur with sufficient margin above the wind tunnel test condition and the static aeroelastic results suggest up to 18% increase in lift-curve slope can be achieved.

Acknowledgements

This research is conducted as part of the project titled: Rear End Aerodynamic and Aeroelastic Studies (Grant Agreement No: 864290). The partners in this project are Airbus, University of Nottingham, University of Bristol and University of Glasgow.

References

[1]Lomax, T. L. "Horizontal Tail Loads," *Structural Loads Analysis for Commercial Transport Aircraft*. American Institute of Aeronautics and Astronautics, Reston, VA, 1996, pp. 115-142.

[2]Shirk, M. H., Hertz, T. J., and Weisshaar, T. A. "Aeroelastic tailoring-theory, practice, and promise," *Journal of Aircraft* Vol. 23, No. 1, 1986, pp. 6-18.

[3]Kim, T.-U., and Hwang, I. H. "Optimal design of composite wing subjected to gust loads," *Computers & Structures* Vol. 83, No. 19, 2005, pp. 1546-1554.doi: https://doi.org/10.1016/j.compstruc.2005.02.002

[4]Weisshaar, T. A., and Duke, D. K. "Induced Drag Reduction Using Aeroelastic Tailoring with Adaptive Control Surfaces," *Journal of Aircraft* Vol. 43, No. 1, 2006, pp. 157-164.doi: 10.2514/1.12040

[5]Rodden, W. P., and Johnson, E. H. *MSC/NASTRAN aeroelastic analysis: user's guide; Version 68*. Los Angeles: MacNeal-Schwendler Corporation, 1994.

[6]Tsai, S. W., "Strength Characteristics of Composite Materials",NASA CR-224, 1965